HHS Public Access

Author manuscript

Biomech Model Mechanobiol. Author manuscript; available in PMC 2020 February 01.

Published in final edited form as:

Biomech Model Mechanobiol. 2019 February ; 18(1): 261–273. doi:10.1007/s10237-018-1080-1.

Absence of LTBP-3 Attenuates the Aneurysmal Phenotype But Not Spinal Effects on the Aorta in Marfan Syndrome

A. Korneva[#1], **L. Zilberberg**[#2], **D.B. Rifkin**[2], **J.D. Humphrey**[1,3], and **C. Bellini**[4,†]

[1]Department of Biomedical Engineering Yale University, New Haven, CT, USA

[2]Departments of Cell Biology and Medicine New York University, New York, NY, USA

[3]Vascular Biology and Therapeutics Program Yale School of Medicine, New Haven, CT, USA

[4]Department of Bioengineering Northeastern University, Boston, MA, USA

[#] These authors contributed equally to this work.

Abstract

Fibrillin-1 is an elastin-associated glycoprotein that contributes to the long term fatigue resistance of elastic fibers as well as to the bioavailability of transforming growth factor-beta (TGFβ) in arteries. Altered TGFβ bioavailability and/or signaling have been implicated in aneurysm development in Marfan syndrome (MFS), a multi-system condition resulting from mutations to the gene that encodes fibrillin-1. We recently showed that absence of the latent transforming growth factor beta binding protein-3 (LTBP-3) in fibrillin-1 deficient mice attenuates the fragmentation of elastic fibers and focal dilatations that are characteristic of aortic root aneurysms in MFS mice, at least to 12 weeks of age. Here, we show further that absence of LTBP-3 in this MFS mouse model improves the circumferential mechanical properties of the thoracic aorta, which appears to be fundamental in preventing or significantly delaying aneurysm development. Yet, a spinal deformity either remains or is exacerbated in the absence of LTBP-3 and seems to adversely affect the axial mechanical properties of the thoracic aorta, thus decreasing overall vascular function despite the absence of aneurysmal dilatation. Importantly, because of the smaller size of mice lacking LTBP-3, allometric scaling facilitates proper interpretation of aortic dimensions and thus the clinical phenotype. While this study demonstrates that LTBP-3/TGFβ directly affects the biomechanical function of the thoracic aorta, it highlights that spinal deformities in MFS might indirectly and adversely affect the overall aortic phenotype. There is a need, therefore, to consider together the vascular and skeletal effects in this syndromic disease.

Keywords

fibrillin-1; aortic stiffness; vascular phenotype; kyphosis; aortic curvature; allometric scaling

[†]Address for correspondence: Chiara Bellini, Ph.D., Department of Bioengineering, Northeastern University, Boston, MA, USA, c.bellini@northeastern.edu +1-617-373-2550.

CONFLICTS OF INTEREST

None to disclose.

INTRODUCTION

Marfan syndrome (MFS) is an autosomal dominant disorder of connective tissues that predisposes affected individuals to, among other conditions, the development of thoracic aortic aneurysm (TAA) and abnormal spinal curvature. MFS is caused by mutations to the gene (*FBN1*) that encodes the extracellular matrix glycoprotein fibrillin-1 (Dietz et al. 2005; Ramirez and Dietz 2004), the primary elastin-associated microfibril found in elastic fibers. Fibrillin-1 contributes to the long-term biomechanical stability of the elastic fibers (Marque et al. 2001; Pereira et al. 1999) as well as to the bioavailability of transforming growth factor beta (TGFβ) within the matrix (Robertson and Rifkin 2016). The latter is accomplished by mediating the incorporation of the TGFβ large latent complex within the matrix, where a latent TGFβ binding protein (LTBP) covalently binds a small latent complex consisting of TGFβ and a TGFβ propeptide (Neptune et al. 2003). The combination of a compromised fatigue resistance of the elastic fibers and altered TGFβ signaling due to abnormal fibrillin-1 is thought to contribute to aneurysmal initiation and progression in MFS.

Several mouse models have been established either to prevent (Carta et al. 2006) or to alter (Judge et al. 2004; Pereira et al. 1999) the expression of fibrillin-1. Mice lacking the fibrillin-1 gene (*Fbn1*$^{-/-}$) are useful for investigating the role of this glycoprotein in organogenesis and elucidating interactions between fibrillin-1 and LTBPs. In particular, we have shown that incorporation of LTBP-3 within the extracellular matrix depends upon fibrillin-1 (Zilberberg et al. 2012). Due to their limited life span (< 2 weeks), however, *Fbn1*$^{-/-}$ mice do not recapitulate the clinical progression of symptoms in MFS. In contrast, hypomorphic *Fbn1*$^{mgR/mgR}$ mice express ~15–20% of the normal amount of fibrillin-1 and exhibit salient features of the lethal adult form of MFS (Pereira et al. 1999). We previously characterized the biaxial mechanical behavior of the ascending (ATA) and descending (DTA) thoracic aorta and common carotid arteries from 8- to 10-week old *Fbn1*$^{mgR/mgR}$ mice (Bellini et al. 2016; Eberth et al. 2009; Ferruzzi et al. 2011). These arteries exhibit decreases in axial (pre)stretch and increases in circumferential material stiffness, both of which contribute to a reduced ability to store elastic energy during systolic deformation. Importantly, the most dramatic biomechanical differences are found near the aortic root and in the proximal ATA, where aneurysms tend to arise, and similar features are observed in this segment across multiple mouse models of TAA (Bellini et al. 2017a).

Recently, we generated *Fbn1*$^{mgR/mgR}$:*Ltbp3*$^{-/-}$ mice to evaluate the roles of LTBP-3 protein in the progression of MFS (Zilberberg et al. 2015). Deletion of the gene *Ltbp3* in *Fbn1*$^{mgR/mgR}$ mice normalized nearly all changes in gene expression characteristic of MFS (i.e., reversed 773 out of the 786 differentially expressed genes), restored the level of TGFβ signaling to normal (as evaluated via pSmad3 protein), and maintained the histological integrity of the elastic fibers, which presumably contributed to the markedly improved survival of these double mutant mice up to 12 weeks of age. Here, we biomechanically phenotype the ATA and DTA from *Ltbp3*$^{-/-}$ and *Fbn1*$^{mgR/mgR}$:*Ltbp3*$^{-/-}$ mice to quantify consequences of the deletion of the *Ltbp3* gene on the overall mechanical functionality and structural integrity of the aneurysm-prone thoracic aorta. Because rigorous biomechanical phenotyping requires biaxial mechanical data – circumferential and axial – we also explored possible relations between spinal deformities and aortic properties, noting that skeletal

development influences the degree of axial (pre)stretch in the aorta (Dobrin et al. 1975; Huang et al. 2006) and possibly its curvature.

METHODS

All animal procedures conformed with NIH guidelines and were approved by the Institutional Animal Care and Use Committee at New York University School of Medicine. All biomechanical testing and data analysis was performed consistent with established methods (Bellini et al. 2017a; Ferruzzi et al. 2013), which enabled our new data for 8–9 week old male *Ltbp3*$^{-/-}$ (n = 5–7) and *Fbn1*$^{mgR/mgR}$:*Ltbp3*$^{-/-}$ (n = 6) mice to be compared directly with previous results on 8–9 week old male wild-type (*WT*, n = 5) and *Fbn1*$^{mgR/mgR}$ (n = 10) mice (Bellini et al. 2016). Note that the colonies of wild- type and mutant mice in both our prior and current work were maintained on a mixed C57BL/6;Sv129;SW genetic background (Zilberberg et al. 2015) within the same facility, and studied mechanically over a 16-month period. Following euthanasia, the ribcage was opened to expose the thoracic aorta from the aortic root to the sixth pair of intercostal arteries. A digital image documented the in situ geometry of the ATA and aortic arch. Following separation from perivascular tissues and gross excision, the proximal and distal thoracic aorta were divided just distal to the left subclavian artery, near the ligamentum arteriosum. Another digital image acquired using a dissection microscope and video camera documented the resulting in vitro geometry prior to preparation for mechanical testing. A curvature index (*CI*) was calculated for the DTA as the ratio of the contour length to the end-to-end distance. Measurements at the inner and outer curvature were averaged, with higher values of indicating greater deviations of the unloaded configuration from a straight line.

In preparation for in vitro mechanical testing, the ATA and proximal DTA were cannulated and placed within our custom computer-controlled testing device (Gleason et al. 2004) within a Hank's buffered physiologic solution maintained at 37°C. The vessels were preconditioned mechanically via cyclic pressurization, while held at their individual in vivo axial length, and then subjected to a series of seven biaxial protocols: cyclic pressurization from ~10 to 140 mmHg at three different values of axial stretch (95, 100, and 105% of the in vivo value) plus cyclic axial stretching at four different fixed values of luminal pressure (10, 60, 100, or 140 mmHg). The associated pressure-diameter and axial force-length data were fit via nonlinear regression of biaxial data from the unloading portions of all seven testing protocols using a validated 8-parameter nonlinear stored energy function (Bellini et al. 2017a; Ferruzzi et al. 2013). This function accounts for the isotropic contribution of an elastin-dominated amorphous matrix (via a neo-Hookean form of stored energy) and anisotropic contributions due to multiple families of locally parallel collagen fibers and circumferentially-oriented passive smooth muscle (via Fung-type exponential forms of stored energy), namely

$$W\left(\mathbf{C},\mathbf{M}^j\right)=\frac{c}{2}\left(I_{\mathbf{C}}-3\right)+\sum_{i=1}^{4}\frac{c_1^i}{4c_2^i}\left\{\exp\left[c_2^i\left(IV_{\mathbf{C}}^i-1\right)^2\right]-1\right\}, \quad (1)$$

where $I_C = tr(\boldsymbol{C})$ and $IV^i_{\mathbf{C}} = \mathbf{M}^i \cdot \mathbf{C}\mathbf{M}^i$ are coordinate invariant measures of the finite deformation, with the right Cauchy-Green tensor $\mathbf{C} = \mathbf{F}^T\mathbf{F}$ computed from the deformation gradient tensor $\mathbf{F}$ that was inferred directly from experimental measurements of changes in diameter and length, with $det\mathbf{F} = 1$ because of assumed incompressibility. The direction of the i^{th}, family of fibers in the traction-free reference configuration was given by the vector $\mathbf{M}^i = \left[0, \sin\alpha_0^i, \cos\alpha_0^i\right]$, with angle α_0^i defined relative to the axial direction. Based on prior microstructural observations for wild-type and fibrillin-1 deficient elastic arteries (Ferruzzi et al. 2011), and the yet unquantified effects of copious cross-links amongst the multiple families of fibers, we included contributions of axial ($\alpha_0^1 = 0$), circumferential ($\alpha_0^2 = \pi/2$), and two symmetric diagonal families of fibers ($\alpha_0^{3,4} = \pm\alpha_0$). Hence, the eight model parameters determined from nonlinear regression of data are: c, c_1^1, c_2^1, c_1^2, c_2^2, $c_1^{3,4}$, $c_2^{3,4}$, and α_0. Values of biaxial stress and material stiffness were computed through appropriate differentiation of the stored energy function, then compared at physiologic pressures and individual values of the in vivo axial stretch using an analysis of variance (ANOVA), with Bonferroni post-hoc testing and $p < 0.05$ considered significant. Experimental data and computational results are presented as mean ± SEM. Horizontal bars in vertical scatter plots identify, from bottom to top, the 25th, 50th (median), and 75th percentiles.

Finally, whole-body CT scans were acquired for additional mice in each of the four groups ($n = 12$ total) using a Siemens Inveon™ micro-PET/CT scanner equipped with an 80-W, 35- to 80-kVp tungsten-anode X-ray source. Euthanized mice were laid in a prone position and scanned at 360° with a continuous rotation in 1° steps. The field of view yielded a spatial resolution of 40 μm. Cross-sectional images were saved in a proprietary format, opened in Fiji (NIH) using the Bio-Formats plug-in, and exported as an image sequence of bitmap files with retained spatial resolution. The z-stack of images was imported into Mimics (Materialise, NV) and segmented using a combination of thresholding and a region-growing algorithm to create a 3D model of the skeleton. The degree of spinal deformity was quantified using dorsal-ventral asymmetries in the length of the spine between thoracic vertebra T4 and lumbar vertebra L6 (Li et al. 2017). Lengths of the dorsal and ventral vertebral aspects were measured in the midsagittal plane using Mimics. Increased differences between dorsal and ventral lengths of the spine arise in kyphosis due to ventral wedging of the vertebral bodies (Li et al. 2017). Unlike graphical methods that estimate the severity of spinal deformity by measuring the angle between the endplates of the most tilted vertebrae (Cobb's angle), the chosen approach is independent of the position assumed by the mice during image acquisition and is thus insensitive to postural adjustments occurring post-mortem due to any change in muscle tone (Stephens et al. 2015).

RESULTS

Ascending Aorta.

The configuration assumed in situ by the ATA appeared similar across all four genotypes (Figure 1, panels A-E), even in the 7 (out of 10) *Fbn1*$^{mgR/mgR}$ mice that developed an aneurysmal dilatation near the aortic root (panel D, mean diameter 76% greater than

normal). Following excision and immersion in physiologic solution, however, the main branches off the aortic arch rearranged naturally to an orientation that differed in all three of the groups with fibrillin-1 deficiency (panels H-J) relative to that for the control (panel F) and *Ltbp3*$^{-/-}$ (panel G) mice. The ATA in mice without LTBP-3 protein (panels G and J) appeared slightly wider (although much less than a 50% increase in diameter, the usual threshold defining an aneurysm) relative to controls (panel F) despite a significantly lower body mass than for both control (23.2±1.5g for *Ltbp3*$^{-/-}$ *vs.* 29.2±0.4g for WT) and fibrillin-1 deficient (21.9±1.5g for *Fbn1*$^{mgR/mgR}$:*Ltbp3*$^{-/-}$ *vs.* 28.8±1.0g for all *Fbn1*$^{mgR/mgR}$) mice. Although one may normalize aortic diameter by body mass (panel K), increases in aortic size follow allometric, not isometric, scaling laws (Supplemental Figure S1, panel B), whereby inner diameter $\hat{d} = \alpha \cdot M^{\beta}$ with M body mass and α and β parameters (West et al. 1997). A logarithmic transformation and linear regression of systolic data (Supplemental Figure S1, panel A) yielded best-fit values of $\alpha = 936.17\ \mu m \cdot g^{-0.17}$ and $\beta = 0.17$ for $n = 21$ control ATAs that were mined from a prior study on adult wild-type male mice with different backgrounds: C57BL/6, C57BL/6;129SvJ, and C57BL/6;129SvEv (Bellini et al. 2017b). Normalizing mouse-specific inner diameter $d_{P_{sys}}$ at transmural pressure P = 120 mmHg by body mass = (Figure 1, panel K) or more appropriately by a normal diameter predicted by allometric scaling ($\hat{d}_{P_{sys}} = 936.17 \cdot M^{0.17}$, panel L) thus enables consistent comparisons of aortic size independent of body mass, whereby it is seen that absence of LTBP-3 prevented aneurysmal dilatation in the *Ltbp3*$^{-/-}$ and *Fbn1*$^{mgR/mgR}$:*Ltbp3*$^{-/-}$ mice, at least over the range of body masses (~17–40 g) and ages (8–9 weeks) studied. That is, even when corrected for body mass, only ATAs from the 7 of 10 *Fbn1*$^{mgR/mgR}$ mice that had been classified as aneurysmal upon gross examination were indeed statistically larger than control.

Absence of LTBP-3 alone did not affect the pressure-diameter response of the ATA (Figure 2, panel A) and there was similarly no difference in its circumferential Cauchy stress-stretch behavior (panel B). Structural (panel C) and material (panel D) behaviors in the axial direction were also comparable in the ATA between *Ltbp3*$^{-/-}$ and *WT* mice. Consistent with these observations and implications from the excised configurations (Figure 1, panels F-G), control and *Ltbp3*$^{-/-}$ ATAs exhibited similar values of in vivo axial stretch (Figure 2, panel E): 1.70±0.04 in WT and 1.69±0.05 in *Ltbp3*$^{+/-}$. The 8-parameter nonlinear constitutive relation (Equation 1) provided a good fit for the biaxial pressure-distension / axial force-extension data from all four genotypes and both aortic segments (not shown), confirming prior findings for other mouse models (Bellini et al. 2017a; Ferruzzi et al. 2013). Associated best-fit values of the material parameters are listed in Table 1, noting that values for the ATA were again delineated in *Fbn1*$^{mgR/mgR}$ mice based on the presence or absence of an aneurysm (> 50% increase in diameter) or allometric scaling. These group-specific constitutive descriptors enabled calculation of the intrinsic (material) biaxial stiffness and the elastic energy stored upon deformation. There were no significant differences in circumferential (panel F) or axial (panel G) material stiffness or stored elastic energy (panel H) between WT and *Ltbp3*$^{-/-}$ mice within the physiological range of pressures considered.

Reduced expression of fibrillin-1 in *Fbn1*$^{mgR/mgR}$ mice is thought to increase mechanical fatigue-induced fragmentation of the associated elastic fibers (Bellini et al. 2016; Pereira et al. 1999). Decreased competency of elastic fibers, in turn, inevitably leads to a straightening of initially undulated collagen fibers at moderate not just high pressures (Ferruzzi et al. 2011), as reflected by the change in shape of the pressure-diameter response (Figure 2, panel A). Perhaps in an attempt to contain the value of circumferential stress below the failure level, the ATA begins to dilate locally in *Fbn1*$^{mgR/mgR}$ mice, eventually becoming aneurysmal near the aortic root (Bellini et al. 2016). Remarkably, absence of LTBP-3 nearly restored to normal the pressure-diameter behavior of fibrillin-1 deficient mice (double mutant *Fbn1*$^{mgR/mgR}$:*Ltbp3*$^{-/-}$ mice; panel A), which also restored circumferential distensibility toward normal in the ATA (panel B). Material stiffness in the circumferential direction, which is predictive of the propensity toward or presence of aneurysmal dilatation (Bellini et al. 2017a; Bellini et al. 2016), was also improved significantly in fibrillin-1 deficiency in the absence of LTBP-3 protein (panel F).

Yet, structural (Figure 2, panel C) and material (panel D) behaviors in the axial direction did not improve in the *Fbn1*$^{mgR/mgR}$:*Ltbp3*$^{-/-}$ ATA when compared to those of the *Fbn1*$^{mgR/mgR}$ ATA. Whereas a progressive loss of elastic fiber integrity in the *Fbn1*$^{mgR/mgR}$ aorta may favor lengthening of the artery as opposed to axial stretching throughout somatic growth, absence of LTBP-3 did not rescue the values of in vivo axial stretch in the *Fbn1*$^{mgR/mgR}$:*Ltbp3*$^{-/-}$ aorta relative to those of the aneurysmal *Fbn1*$^{mgR/mgR}$ ATA, despite the absence of elastic fiber fragmentation in double mutant aortas (cf. Figure 1, panels D and E in (Zilberberg et al. 2015)). Values of the in vivo axial stretch were 1.42±0.06 in aneurysmal *Fbn1*$^{mgR/mgR}$ and 1.41±0.02 in *Fbn1*$^{mgR/mgR}$:*Ltbp3*$^{-/-}$ mice, each compared to 1.70±0.04 in WT mice (panel E). Given the documented integrity of the elastic fibers in double mutant aortas and lack of a marked deposition of other matrix proteins (Zilberberg et al. 2015), the source of this decrease in axial stretch should be sought other than from the microstructure. Hence, recall that the excised *Fbn1*$^{mgR/mgR}$:*Ltbp3*$^{-/-}$ ATA was closer in shape to the *Fbn1*$^{mgR/mgR}$ than to either the WT or the *Ltbp3*$^{-/-}$ ATA (Figure 1, panels F-J). Despite the decrease in the in vivo axial stretch, fibrillin-1 deficiency, either alone or combined with absent LTBP-3, did not alter significantly the axial material stiffness at physiological levels of pressure (Figure 2, panel G), which suggests some compensatory adaptation by the wall.

A key function of the aorta is to store elastic energy during systole and to use this energy during diastole to augment blood flow. Energy storage is significantly lower in the ATA of *Fbn1*$^{mgR/mgR}$ mice, with or without aneurysm (Figure 2, panel H); see, too, the isoenergy contour plots that reveal the dependence of energy storage on biaxial deformations (Supplemental Figure S3). Importantly, the energy stored by the ATA of *Fbn1*$^{mgR/mgR}$:*Ltbp3*$^{-/-}$ mice, over a physiological range of pressure, was intermediate between *WT* and *Fbn1*$^{mgR/mgR}$ values, though closer to the non-aneurysmal fibrillin-1 deficient vessels (Figure 2, panel H). Together, these findings suggest that reduced values of axial (pre)stretching compromise aortic function, even if circumferential wall properties are largely preserved.

Descending Thoracic Aorta.

The proximal segment of the DTA remained fairly straight upon removal from WT mice (curvature index $CI = 1.01 \pm 0.003$; Figure 3, panel A). Absence of LTBP-3 alone changed the unloaded configuration of the DTA only slightly (($CI = 1.03 \pm 0.008$; panel B) while there was a marked curvature in the DTAs harvested from fibrillin-1 deficient mice ($CI = 1.07 \pm 0.009$; panel C). Interestingly, this increased curvature was also pronounced in the DTA from the double mutant $Fbn1^{mgR/mgR}$:$Ltbp3^{-/-}$ mice ($CI = 1.06 \pm 0.008$; panel D), suggesting again that absence of LTBP-3 does not improve the axial behavior in MFS.

Absence of LTBP-3 alone again did not affect the pressure-diameter response (Figure 3, panel E) and there was no difference in the circumferential Cauchy stress-stretch behavior relative to control (panel F). There was, however, a slight decrease in axial extensibility in the $Ltbp3^{-/-}$ DTA (panels G and H). Consistent with these observations, there was a trend toward a reduced axial stretch in the $Ltbp3^{-/-}$ DTA relative to control (panel I): 1.60±0.05 in WT vs. 1.54±0.03 in $Ltbp3^{-/-}$. Yet, there were no significant differences in circumferential (panel J) or axial (panel K) material stiffness or stored elastic energy (panel L) between the WT and $Ltbp3^{-/-}$ DTA within the physiological range of pressures considered. Absence of LTBP-3 also improved the pressure-diameter behavior in the DTA of fibrillin-1 deficient mice (panel E), with preserved circumferential distensibility (panel F) though not axial extensibility (panels G and H). Indeed, structural (panel G) and material (panel H) behaviors in the axial direction did not improve in the $Fbn1^{mgR/mgR}$:$Ltbp3^{-/-}$ aorta when compared to the $Fbn1^{mgR/mgR}$ aorta. Absence of LTBP-3 also did not rescue values of the in vivo axial stretch in the $Fbn1^{mgR/mgR}$:$Ltbp3^{-/-}$ DTA relative to those in $Fbn1^{mgR/mgR}$, with values of 1.44±0.03 in the $Fbn1^{mgR/mgR}$:$Ltbp3^{-/-}$ mice and 1.45±0.03 in the $Fbn1^{mgR/mgR}$ mice, each compared to 1.60±0.05 in WT mice (panel I). Given that the excised $Ltbp3^{-/-}$, $Fbn1^{mgR/mgR}$, and $Fbn1^{mgR/mgR}$:$Ltbp3^{-/-}$ DTAs all assumed a curved shape, though to different extents, and recalling the physical connection between the thoracic aorta and the spine, there was strong motivation to quantify spinal curvature.

Spinal Deformity.

Absence of LTBP-3 and deficiency of fibrillin-1 both cause deformities in the thoracic spine (Dabovic et al. 2002a; Dabovic et al. 2002b), which could be responsible, at least in part, for the curvature of the aortic segments that are supported directly by the thoracic vertebrae throughout somatic growth (Dobrin 1997; Nathan 1988). The curvature of the spine in the sagittal plane (Figure 4, panels A-D) was quantified through ventral wedging (panel G), a site-specific difference in length between the dorsal (panel E) and ventral (panel F) aspects of the vertebrae. The spine of WT mice displayed a natural kyphotic (convex) curve between the thoracic vertebrae T7 and T13, which was only slightly amplified in $Ltbp3^{-/-}$ mice at T13 (panel G). Thoracic kyphosis was exacerbated in $Fbn1^{mgR/mgR}$ mice between the thoracic vertebrae T9 and T13, with the maximum at T12 (panel G). Consistently, the double mutation did not rescue, but rather maintained, the severe kyphosis seen in the $Fbn1^{mgR/mgR}$ mice (panel G). Importantly, there was a strong correlation (panel J) between the measured residual curvature index (Figure 3, panels A-D) for the excised DTA (Figure 4, panel H) and the maximum value of vertebral wedging (panel I), consistent with a strong spinal influence on growth of the descending thoracic aorta.

DISCUSSION

Altered TGFβ signaling has been suggested to contribute to the development of TAAs in patients with MFS (*FBN1* mutation; (Neptune et al. 2003)) and Loeys-Dietz syndrome (*TGFBR1* or *TGFBR2* mutation; (Loeys et al. 2005; Maleszewski et al. 2009)). Altered TGFβ signaling has also been observed in patients with a familial predisposition to TAAs (*MYH11* and *ACTA2* mutations; (Renard et al. 2013)) and in rare connective tissue disorders associated with arterial tortuosity and aneurysms, including *cutis laxa* syndrome (*FBLN4* mutation; (Renard et al. 2010)) and arterial tortuosity syndrome (*SLC2A10* mutation; (Coucke et al. 2006)). Defective sequestration of and consequent altered bioavailability of TGFβ in MFS can result from a faulty interaction between abnormal fibrillin-1 microfibrils and the large latent TGFβ complex, with the small latent TGFβ complex covalently bound to a LTBP (Ramirez and Dietz 2004; Robertson and Rifkin 2016). Specifically, using tissue preparations and cell cultures from $Fbn1^{-/-}$ mice, we previously showed that LTBP-3 is not incorporated into extracellular matrix lacking fibrillin-1 (Zilberberg et al. 2012). We also observed an increase in the survival rate, up to 12 weeks of age, of $Fbn1^{mgR/mgR}$:$Ltbp3^{-/-}$ mice compared with $Fbn1^{mgR/mgR}$ mice, with reduced elastic fiber fragmentation, reduced differentially expressed genes, normalized TGFβ signaling, and lack of gross TAAs in the compound mutants (Zilberberg et al. 2015). Neither structural nor mechanical consequences of LTBP-3/FBN1 interactions had been examined before, however.

Here we performed a consistent biaxial mechanical characterization of the ascending and proximal descending thoracic aortas from $Ltbp3^{-/-}$ and $Fbn1^{mgR/mgR}$:$Ltbp3^{-/-}$ mice and compared results with prior data from WT and $Fbn1^{mgR/mgR}$ aortas, all with a similar mixed genetic background and maintained in the same colony. Importantly, we previously found an increase in circumferential material stiffness and a decrease in circumferential distensibility of the thoracic aorta in fibrillin-1 deficiency (Bellini et al. 2016), with the degree of changes correlating with aneurysmal propensity and severity (Bellini et al. 2017a). Consistent with the improved survival rate and lack of aneurysm, thoracic aortas from 8–9 week old male $Fbn1^{mgR/mgR}$:$Ltbp3^{-/-}$ mice showed near normal circumferential material and structural responses over a physiological range of pressurization and axial stretch (Figure 2, panels A-D; Figure 3, panels E-H). This finding suggests that absence of LTBP-3 prevents or delays pathological effects of LTBP-3/TGFβ complexes in aneurysmal development in MFS mice, at least up to 12 weeks of age (Zilberberg et al. 2015). At higher pressures, however, the circumferential direction stiffened slightly more rapidly in the $Ltbp3^{-/-}$, and thus $Fbn1^{mgR/mgR}$:$Ltbp3^{-/-}$, thoracic aorta than in the WT aorta (Figure 2, panel F; Figure 3, panel J). Although absence of LTBP-3 appears to favorably alter physiological TGFβ signaling in a way that – directly or indirectly – allows or facilitates normal development and maintenance of aortic tissue (e.g., near normal pSmad3 and pERK1/2 as shown by (Zilberberg et al. 2015)), there is yet a need to determine if a similar protection would be afforded in cases of increased mechanical loading, including hypertension, and increased aging.

Of particular note, $Ltbp3^{-/-}$ mice with and without fibrillin-1 deficiency were significantly smaller. Whereas aortic diameter is often normalized in patients using body surface area

(BSA) to account for expected normal differences in diameter with body size (Davies et al. 2006), we are not aware of a previously validated scaling for mice. Although normalization by body mass may seem to be natural (Chen et al. 2017; Guo et al. 2018), aortic growth scales allometrically, not isometrically, with body mass (West et al. 1997), hence it is prudent to use allometric scaling ($\hat{d} = \alpha \cdot M^{\beta}$, with $\alpha > 0$ and $\beta < 1$) to compare aortic diameters across different genotypes (Hayashi and Sugimoto 2007; Matsumoto and Hayashi 1994) or species (Goergen et al. 2007; Greve et al. 2006; Prim et al. 2018). Given that the parameter values for allometric scaling of the inner diameter of the ATA may vary with sex, age, and range of body mass (de Simone et al. 1997), prior data from $n = 21$ age- and sex-matched wild-type mice with similar genetic backgrounds and body mass to those of the mice studied here (~17 to 40 g) were used to identify the two model parameters. Figure 1 (panels K and L) shows that absence of LTBP-3 led to a non-significant increase in diameter (normalized either by body mass M or by the theoretical normal value of diameter predicted by allometric scaling, $\hat{d} = \alpha \cdot M^{\beta}$), while protecting against the aneurysmal dilatation that was otherwise seen in 70% of the $Fbn1^{mgR/mgR}$ mice at 8–9 weeks of age. This protection is consistent with the nearly restored circumferential properties and improved, but not restored, elastic energy storage. The degree of axial extension typically plays an important role in such energy storage.

It is well known that the aorta (and all central arteries) retracts upon excision, thus revealing the existence of an axial (pre)stretch. This axial stretching enables the aorta to function at an energetically favorable length at which changes in blood pressure do not change the axial force (Humphrey et al. 2009; Van Loon 1977). Although absence of LTBP-3 did not alter the axial behavior of the ATA, it led to a modest decrease in the in vivo axial stretch of the DTA (Figure 2, panel E vs. Figure 3, panel I). This regional dependence could reflect differences in either smooth muscle cell lineage (neural crest in the ascending vs. mesoderm in the descending thoracic aorta; (Majesky 2007)) or perivascular tethering (Ferruzzi et al. 2018a), as changes in basal TGFβ signaling may influence thoracic organs and tissues – including the spine – that impose physical constraints on the aorta at specific anatomical locations. Recall, therefore, that most murine aortas prone to aneurysmal development, including in $Fbn1^{mgR/mgR}$ mice, exhibit a lower in vivo axial stretch (Bellini et al. 2017a), though this need not be causative. Importantly, a diminished axial stretch was found in the ATA and DTA of $Fbn1^{mgR/mgR}$:$Ltbp3^{-/-}$ mice (Figure 2, panel E and Figure 3, panel I), which likely reduced the energy storage capability (Supplemental Figure S3).

Axial pre-stretch of the aorta appears to arise largely from the perinatal deposition and crosslinking of elastin and subsequent somatic growth (Dobrin et al. 1975; Humphrey et al. 2009). In the DTA, intercostal arteries that originate as lateral branches on both sides force the aorta to follow the curvature of the spine closely (Nathan 1988). This intimate spatial relationship between aorta and spine is maintained in the presence of kyphosis and scoliosis (Edeiken 1933; Liljenqvist et al. 2002; Maruyama et al. 2004; Milbrandt and Sucato 2007; Nathan 1988; Sevastik et al. 1996; Sucato and Duchene 2003). Although it has long been appreciated that the aorta accommodates developing spinal deformities by growing into a curved shape (Edeiken 1933), the concomitant decrease in the in vivo axial stretch and the effect of such structural changes on vascular function had not been quantified previously in

mice, particularly in MFS. To this end, we evaluated the residual curvature of each specimen in the unloaded configuration, which is unique and therefore better suited for comparisons across experimental groups than any loaded configuration wherein body position could vary from mouse to mouse. Both *Fbn1*$^{mgR/mgR}$ and *Ltbp3*$^{-/-}$ mice are commonly affected by kyphosis (Dabovic et al. 2002a; Pereira et al. 1999), which led to changes in the unloaded configuration of the DTA compared to that in control mice (Figure 3, panels A-C). This feature was retained in the DTA from *Fbn1*$^{mgR/mgR}$:*Ltbp3*$^{-/-}$ mice (panel D), though possibly being more severe due to the combined effects of the two mutations. Although the spine is not directly in contact with the ATA, severe spinal deformities can affect the development of the thoracic cavity and rib cage, elevating the aortic arch above the clavicle, thus altering the spatial relationship between the aortic arch and its main branches (Parkinson et al. 1939). The unloaded configuration of the ATA from *Ltbp3*$^{-/-}$ mice was similar to that of control mice despite their spinal deformity (Figure 1, panels F and G). Conversely, the orientation of the main branches off the arch from *Fbn1*$^{mgR/mgR}$ mice was clearly altered, and this feature persisted in the ATA from *Fbn1*$^{mgR/mgR}$:*Ltbp3*$^{-/-}$ mice (Figure 1, panels H-J). Consistently, axial stretch was lower in the ATA from fibrillin-1 deficient mice, even in the absence of LTBP-3 (Figure 2, panel E). In both the ascending and descending regions of the thoracic aorta, a decreased value of in vivo axial stretch impairs cardiovascular function by reducing the elastic energy stored during systolic deformation, even when circumferential properties of the wall remain normal (Figure 2, panel H; Figure 3, panel L; supplemental Figure S3).

Although this study was motivated by the need to characterize biomechanical consequences of previously observed changes in gene expression, histology, cell signaling, and overall survival in *Fbn1*$^{mgR/mgR}$:*Ltbp3*$^{-/-}$ mice (Zilberberg et al. 2015), the recent discovery that pathologic variants in *LTBP3* predispose human subjects to thoracic aortic aneurysms and dissections (Guo et al. 2018) renders the current *Ltbp3*$^{-/-}$ data important as well. Findings in 13 subjects from two families revealed that *LTBP3* variants give rise to myriad disease conditions, including dental anomalies, skeletal disorders, and valvular and arterial defects. Given that these individuals are often of short stature, and presumably have lower than normal body mass, there is yet a need to assess the perceived arterial/aortic dilatation in terms of an appropriate normalization, such as body surface area (Davies et al. 2006). Body surface area is often calculated using a power law formula in terms of body mass and height, each with an exponent $\beta < 1$, which is consistent with allometric scaling. Based on direct allometric scaling of ascending aortas from normal adult male mice with body mass between ~17 and 40 g (cf. Figure 1 and Supplemental Figures S1 and S2), we found that ATA diameter is slightly greater than normal in *Ltbp3*$^{-/-}$ mice, but not significantly so, at least at the ages studied.

Importantly, amongst the many conditions observed in patients with *LTBP3* variants (Guo et al. 2018), aortic dissection was a definitive diagnosis in 3/13. We have previously observed aortic delamination during in vitro biaxial mechanical testing in multiple mouse models wherein dissection manifests in vivo, as, for example, in *Tgfbr2*$^{f/f}$ + tamoxifen (Ferruzzi et al. 2016), *ApoE*$^{-/-}$ + angiotensin II (Bersi et al. 2017), and normally aged (Ferruzzi et al. 2018b) mice, yet we did not observe any aortic delamination during comparable mechanical testing of aortas from *Ltbp3*$^{-/-}$ or *Fbn1*$^{mgR/mgR}$:*Ltbp3*$^{-/-}$ mice. Because biomechanical

mechanisms of dissection are very different from those of aneurysmal dilatation (Bellini et al. 2014; Ferruzzi et al. 2018b), there remains a need to evaluate the mechanics further in these multiple mouse models, particularly in cases of induced hypertension and in older mice. Indeed, differential aortic aging in mice and humans may contribute to inherent differences between mouse models of thoracic aortopathy and actual human disease. We recently found, for example, that normal aortic aging to 100 weeks in C57BL/6;129/SvEv mice manifests primarily as increased intramural collagen and glycosaminoglycans, with largely preserved elastic lamellar structures and function (Ferruzzi et al. 2018b). Humans, on the other hand, experience progressive aging-induced mechanical fatigue of elastic fibers over decades (O'Rourke and Hashimoto 2007), which can exacerbate compromised elastic fiber integrity resulting from genetic mutations. Because fatigue-induced damage to elastic fibers can contribute to aneurysmal dilatation (Wilson et al. 2012), mouse models cannot phenocopy exactly such a progressive process. Note, therefore, that the age of presentation of aortic aneurysm ranged from 34 to 54 in patients with homozygous *LTBP3* variants and 74 to 84 in those with heterozygous variants (Guo et al. 2018). Age-related effects on elastic fibers could contribute to the fundamental difference between our findings in $Ltbp3^{-/-}$ and $Fbn1^{mgR/mgR}$:$Ltbp3^{-/-}$ mice and humans with pathologic *LTBP3* variants.

In summary, our mechanical characterization of the thoracic aorta from $Fbn1^{mgR/mgR}$:$Ltbp3^{-/-}$ mice supports the concept that LTBP-3/TGFβ complexes contribute to the progression of thoracic aortopathy in a mouse model of MFS. Whether LTBP-3 has a direct, or indirect, structural role is not known, but the present data reveal clearly that absence of LTBP-3 protein in a mouse model of fibrillin-1 deficiency yields a normal level of circumferential material stiffness and prevents aneurysmal enlargement, at least over the ages studied. Yet, lack of LTBP-3 does not correct – indeed it may exacerbate slightly – skeletal deformities induced by fibrillin-1 deficiency, which in turn may alter the pattern of physiological axial (pre)stretch developed by the aorta. Due to the strong mechanical coupling between circumferential and axial behaviors, abnormal aortic curvature and/or a lower values of in vivo axial stretch decrease the amount of elastic energy that the thoracic aortic wall is able to store during systole and use during diastole to work on the blood; that is, overall mechanical functionality is yet compromised. These results further emphasize the importance of biaxial testing and the role of axial stretch in arterial mechanics (Humphrey et al. 2009), as well as potential important couplings between skeletal and vascular development that warrant further research. In syndromic diseases such as MFS, understanding aortic phenotypes and the treatment thereof should include consideration of skeletal phenotypes. Further effort should also be devoted to investigate the mechanical functionality and structural integrity of the aorta in other cases of spinal deformities, and there is a pressing need to consider aortic dilatation within the proper context of body size, with group-specific allometric scaling appropriate for comparisons across different mouse models.

Supplementary Material

Refer to Web version on PubMed Central for supplementary material.

ACKNOWLEGMENTS

We thank Professor F. Ramirez, Mt. Sinai School of Medicine, for thoughtful comments, Professor D.M. Milewicz, University of Texas Medical Center – Houston, for stimulating conversations regarding the need to correct aortic diameter according to body size, and Ms. Arunika Makam for the segmentation of the CT images.

FUNDING

This work was supported, in part, by grants from the NIH (P01 HL134605 to DBR, with Core C to JDH, as well as R01 HL105297 and U01 HL116323 to JDH), and The Marfan Foundation to DBR.

REFERENCES

1. Bellini C et al. (2017a) Comparison of 10 murine models reveals a distinct biomechanical phenotype in thoracic aortic aneurysms J R Soc Interface 14 doi:10.1098/rsif.2016.1036
2. Bellini C, Caulk AW, Li G, Tellides G, Humphrey JD (2017b) Biomechanical phenotyping of the murine aorta: What is the best control? J Biomech Eng 139 doi:10.1115/1.4035551
3. Bellini C, Ferruzzi J, Roccabianca S, Di Martino ES, Humphrey JD (2014) A microstructurally motivated model of arterial wall mechanics with mechanobiological implications Ann Biomed Eng 42:488–502 doi:10.1007/s10439-013-0928-x [PubMed: 24197802]
4. Bellini C, Korneva A, Zilberberg L, Ramirez F, Rifkin DB, Humphrey JD (2016) Differential ascending and descending aortic mechanics parallel aneurysmal propensity in a mouse model of Marfan syndrome J Biomech 49:2383–2389 doi:10.1016/j.jbiomech.2015.11.059 [PubMed: 26755343]
5. Bersi MR, Khosravi R, Wujciak AJ, Harrison DG, Humphrey JD (2017) Differential cell-matrix mechanoadaptations and inflammation drive regional propensities to aortic fibrosis, aneurysm or dissection in hypertension J R Soc Interface 14 doi:10.1098/rsif.2017.0327
6. Carta L et al. (2006) Fibrillins 1 and 2 perform partially overlapping functions during aortic development J Biol Chem 281:8016–8023 doi:10.1074/jbc.M511599200 [PubMed: 16407178]
7. Chen J et al. (2017) Loss of smooth muscle α-actin leads to NF-κB-dependent increased sensitivity to angiotensin II in smooth muscle cells and aortic enlargement Circulation Research 120 1903–1915 doi 10.1161/circresaha.117.310563 [PubMed: 28461455]
8. Coucke PJ et al. (2006) Mutations in the facilitative glucose transporter GLUT10 alter angiogenesis and cause arterial tortuosity syndrome Nat Genet 38:452 doi:10.1038/ng1764 [PubMed: 16550171]
9. Dabovic B, Chen Y, Colarossi C, Obata H, Zambuto L, Perle MA, Rifkin DB (2002a) Bone abnormalities in latent TGF-β binding protein (Ltbp)-3–null mice indicate a role for Ltbp-3 in modulating TGF-β bioavailability J Cell Biol 156:227–232 doi:10.1083/jcb.200111080 [PubMed: 11790802]
10. Dabovic B, Chen Y, Colarossi C, Zambuto L, Obata H, Rifkin D (2002b) Bone defects in latent TGF-beta binding protein (Ltbp)-3 null mice; a role for Ltbp in TGF-beta presentation J Endocrinol 175:129–141 doi:10.1677/joe.0.1750129 [PubMed: 12379497]
11. Davies RR et al. (2006) Novel measurement of relative aortic size predicts rupture of thoracic aortic aneurysms Ann Thorac Surg 81:169–177 doi:10.1016/j.athoracsur.2005.06.026 [PubMed: 16368358]
12. de Simone G et al. (1997) Stroke volume and cardiac output in normotensive children and adults. Assessment of relations with body size and impact of overweight Circulation 95:1837–1843 [PubMed: 9107171]
13. Dietz HC, Loeys B, Carta L, Ramirez F (2005) Recent progress towards a molecular understanding of Marfan syndrome Am J Med Genet C Semin Med Genet 139C:4–9 doi:10.1002/ajmg.c.30068 [PubMed: 16273535]
14. Dobrin P, Canfield T, Sinha S (1975) Development of longitudinal retraction of carotid arteries in neonatal dogs Experientia 31:1295–1296 [PubMed: 1204778]
15. Dobrin PB (1997) Physiology and pathophysiology of blood vessels In: Sidawy AN, Sunipio BE, DePalma RG (eds) The basic science of vascular disease. Futura Publishing, New York, pp 69–105

16. Eberth JF, Taucer AI, Wilson E, Humphrey JD (2009) Mechanics of carotid arteries in a mouse model of Marfan Syndrome Ann Biomed Eng 37:1093–1104 doi:10.1007/s10439-009-9686-1 [PubMed: 19350391]
17. Edeiken J (1933) The effect of spinal deformities on the heart Am J Med Sci 8:862–863 doi: 10.1016/S0002-8703(33)90158-1
18. Ferruzzi J, Bersi MR, Humphrey JD (2013) Biomechanical phenotyping of central arteries in health and disease: advantages of and methods for murine models Ann Biomed Eng 41:1311–1330 doi:10.1007/s10439-013-0799-1 [PubMed: 23549898]
19. Ferruzzi J, Collins MJ, Yeh AT, Humphrey JD (2011) Mechanical assessment of elastin integrity in fibrillin-1-deficient carotid arteries: implications for Marfan syndrome Cardiovasc Res 92:287–295 doi:10.1093/cvr/cvr195 [PubMed: 21730037]
20. Ferruzzi J, Di Achille P, Tellides G, Humphrey JD (2018a) Combining in vivo and in vitro biomechanical data reveals key roles of perivascular tethering in central artery function PLOS ONE 13:e0201379 doi:10.1371/journal.pone.0201379 [PubMed: 30192758]
21. Ferruzzi J, Madziva D, Caulk AW, Tellides G, Humphrey JD (2018b) Compromised mechanical homeostasis in arterial aging and associated cardiovascular consequences Biomech Model Mechanobiol 17 1281–1295 doi 10.1007/s10237-018-1026-7
22. Ferruzzi J et al. (2016) Pharmacologically improved contractility protects against aortic dissection in mice with disrupted transforming growth factor-beta signaling despite compromised extracellular matrix properties Arterioscler Thromb Vasc Biol 36:919–927 doi:10.1161/ ATVBAHA.116.307436 [PubMed: 26988590]
23. Gleason RL, Gray SP, Wilson E, Humphrey JD (2004) A multiaxial computer-controlled organ culture and biomechanical device for mouse carotid arteries J Biomech Eng 126:787–795 [PubMed: 15796337]
24. Goergen CJ, Johnson BL, Greve JM, Taylor CA, Zarins CK (2007) Increased anterior abdominal aortic wall motion: Possible role in aneurysm pathogenesis and design of endovascular devices J Endovasc Ther 14:574–584 doi:10.1177/152660280701400421 [PubMed: 17696635]
25. Greve JM et al. (2006) Allometric scaling of wall shear stress from mice to humans: quantification using cine phase-contrast MRI and computational fluid dynamics Am J Physiol Heart Circ Physiol 291:H1700–H1708 doi:10.1152/ajpheart.00274.2006 [PubMed: 16714362]
26. Guo D-C et al. (2018) *LTBP3* pathogenic variants predispose individuals to thoracic aortic aneurysms and dissections Am J Hum Genet 102:706–712 doi:10.1016/j.ajhg.2018.03.002 [PubMed: 29625025]
27. Hayashi K, Sugimoto T (2007) Biomechanical response of arterial wall to DOCA–salt hypertension in growing and middle-aged rats J Biomech 40:1583–1593 doi:10.1016/j.jbiomech. 2006.07.021 [PubMed: 17045273]
28. Huang Y, Guo X, Kassab GS (2006) Axial nonuniformity of geometric and mechanical properties of mouse aorta is increased during postnatal growth Am J Physiol Heart Circ Physiol 290:H657–H664 doi:10.1152/ajpheart.00803.2005 [PubMed: 16172154]
29. Humphrey JD, Eberth JF, Dye WW, Gleason RL (2009) Fundamental role of axial stress in compensatory adaptations by arteries J Biomech 42:1–8 doi:10.1016/j.jbiomech.2008.11.011 [PubMed: 19070860]
30. Judge DP et al. (2004) Evidence for a critical contribution of haploinsufficiency in the complex pathogenesis of Marfan syndrome J Clin Invest 114:172–181 doi:10.1172/JCI20641 [PubMed: 15254584]
31. Li B, Urban JPG, Yu J (2017) Development of spinal deformities in the tight-skin mouse Bone Res 5:16053 doi:10.1038/boneres.2016.53 [PubMed: 28944086]
32. Liljenqvist UR, Allkemper T, Hackenberg L, Link TM, Steinbeck J, Halm HF (2002) Analysis of vertebral morphology in idiopathic scoliosis with use of magnetic resonance imaging and multiplanar reconstruction J Bone Joint Surg Am 84-A:359–368 [PubMed: 11886904]
33. Loeys BL et al. (2005) A syndrome of altered cardiovascular, craniofacial, neurocognitive and skeletal development caused by mutations in TGFBR1 or TGFBR2 Nat Genet 37:275 doi:10.1038/ ng1511 [PubMed: 15731757]

34. Majesky MW (2007) Developmental basis of vascular smooth muscle diversity Arteriosclerosis, Thrombosis, and Vascular Biology 27:1248–1258 doi 10.1161/atvbaha.107.141069
35. Maleszewski JJ, Miller DV, Lu J, Dietz HC, Halushka MK (2009) Histopathologic findings in ascending aortas from individuals with Loeys-Dietz Syndrome (LDS) Am J Surg Pathol 33:194–201 doi:10.1097/PAS.0b013e31817f3661 [PubMed: 18852674]
36. Marque V, Kieffer P, Gayraud B, Lartaud-Idjouadiene I, Ramirez F, Atkinson J (2001) Aortic wall mechanics and composition in a transgenic mouse model of Marfan syndrome Arterioscler Thromb Vasc Biol 21:1184–1189 doi:10.1161/hq0701.092136 [PubMed: 11451749]
37. Maruyama T, Takeshita K, Nakamura K, Kitagawa T (2004) Spatial relations between the vertebral body and the thoracic aorta in adolescent idiopathic scoliosis Spine (Phila Pa 1976) 29:2067–2069 doi:10.1097/01.brs.0000138409.14577.f0 [PubMed: 15371710]
38. Matsumoto T, Hayashi K (1994) Mechanical and dimensional adaptation of rat aorta to hypertension J Biomech Eng 116:278–283 doi:10.1115/1.2895731 [PubMed: 7799628]
39. Milbrandt TA, Sucato DJ (2007) The position of the aorta relative to the spine in patients with left thoracic scoliosis: a comparison with normal patients Spine (Phila Pa 1976) 32:E348–353 doi: 10.1097/BRS.0b013e318059aeda [PubMed: 17515808]
40. Nathan H (1988) Relations of the soft structures of the posterior mediastinum in the scoliotic spine Acta Anat 133:260–264 [PubMed: 3227785]
41. Neptune ER et al. (2003) Dysregulation of TGF-beta activation contributes to pathogenesis in Marfan syndrome Nat Genet 33:407–411 doi:10.1038/ng1116 [PubMed: 12598898]
42. O'Rourke MF, Hashimoto J (2007) Mechanical factors in arterial aging: a clinical perspective J Am Coll Cardiol 50:1–13 doi:10.1016/j.jacc.2006.12.050 [PubMed: 17601538]
43. Parkinson J, Bedford DE, Almond S (1939) The kinked carotid artery that simulates aneurysm Br Heart J 1:345–361 [PubMed: 18609830]
44. Pereira L et al. (1999) Pathogenetic sequence for aneurysm revealed in mice underexpressing fibrillin-1 Proc Natl Acad Sci U S A 96:3819–3823 doi:10.1073/pnas.96.7.3819 [PubMed: 10097121]
45. Prim DA et al. (2018) Comparative mechanics of diverse mammalian carotid arteries PLOS ONE 13:e0202123 doi:10.1371/journal.pone.0202123 [PubMed: 30096185]
46. Ramirez F, Dietz HC (2004) Therapy Insight: aortic aneurysm and dissection in Marfan's syndrome Nat Clin Pract Cardiovasc Med 1:31 doi:10.1038/ncpcardio0020 [PubMed: 16265257]
47. Renard M et al. (2013) Novel MYH11 and ACTA2 mutations reveal a role for enhanced TGFβ signaling in FTAAD Int J Cardiol 165:314–321 doi:10.1016/j.ijcard.2011.08.079 [PubMed: 21937134]
48. Renard M et al. (2010) Altered TGFβ signaling and cardiovascular manifestations in patients with autosomal recessive cutis laxa type I caused by fibulin-4 deficiency Eur J Hum Genet 18:895 doi: 10.1038/ejhg.2010.45 [PubMed: 20389311]
49. Robertson IB, Rifkin DB (2016) Regulation of the bioavailability of TGF-beta and TGF-beta-related proteins Cold Spring Harb Perspect Biol 8 doi:10.1101/cshperspect.a021907
50. Sevastik B, Xiong B, Hedlund R, Sevastik J (1996) The position of the aorta in relation to the vertebra in patients with idiopathic thoracic scoliosis Surg Radiol Anat 18:51–56 [PubMed: 8685813]
51. Stephens RB, Karau KH, Yahnke CJ, Wendt SR, Rowe RJ (2015) Dead mice can grow – variation of standard external mammal measurements from live and three postmortem body states J Mammal 96:185–193 doi:10.1093/jmammal/gyu022
52. Sucato DJ, Duchene C (2003) The position of the aorta relative to the spine: a comparison of patients with and without idiopathic scoliosis J Bone Joint Surg Am 85-A:1461–1469 [PubMed: 12925625]
53. Van Loon P (1977) Length-force and volume-pressure relationships of arteries Biorehology 14:181–201 doi 10.3233/BIR-1977-14405
54. West GB, Brown JH, Enquist BJ (1997) A general model for the origin of allometric scaling laws in biology Science 276:122 doi:10.1126/science.276.5309.122 [PubMed: 9082983]

55. Wilson JS, Baek S, Humphrey JD (2012) Importance of initial aortic properties on the evolving regional anisotropy, stiffness and wall thickness of human abdominal aortic aneurysms J R Soc Interface 9:2047–2058 doi:10.1098/rsif.2012.0097 [PubMed: 22491975]

56. Zilberberg L, Phoon CK, Robertson I, Dabovic B, Ramirez F, Rifkin DB (2015) Genetic analysis of the contribution of LTBP-3 to thoracic aneurysm in Marfan syndrome Proc Natl Acad Sci U S A 112:14012–14017 doi:10.1073/pnas.1507652112 [PubMed: 26494287]

57. Zilberberg L, Todorovic V, Dabovic B, Horiguchi M, Courousse T, Sakai LY, Rifkin DB (2012) Specificity of latent TGF-beta binding protein (LTBP) incorporation into matrix: role of fibrillins and fibronectin J Cell Physiol 227:3828–3836 doi:10.1002/jcp.24094 [PubMed: 22495824]

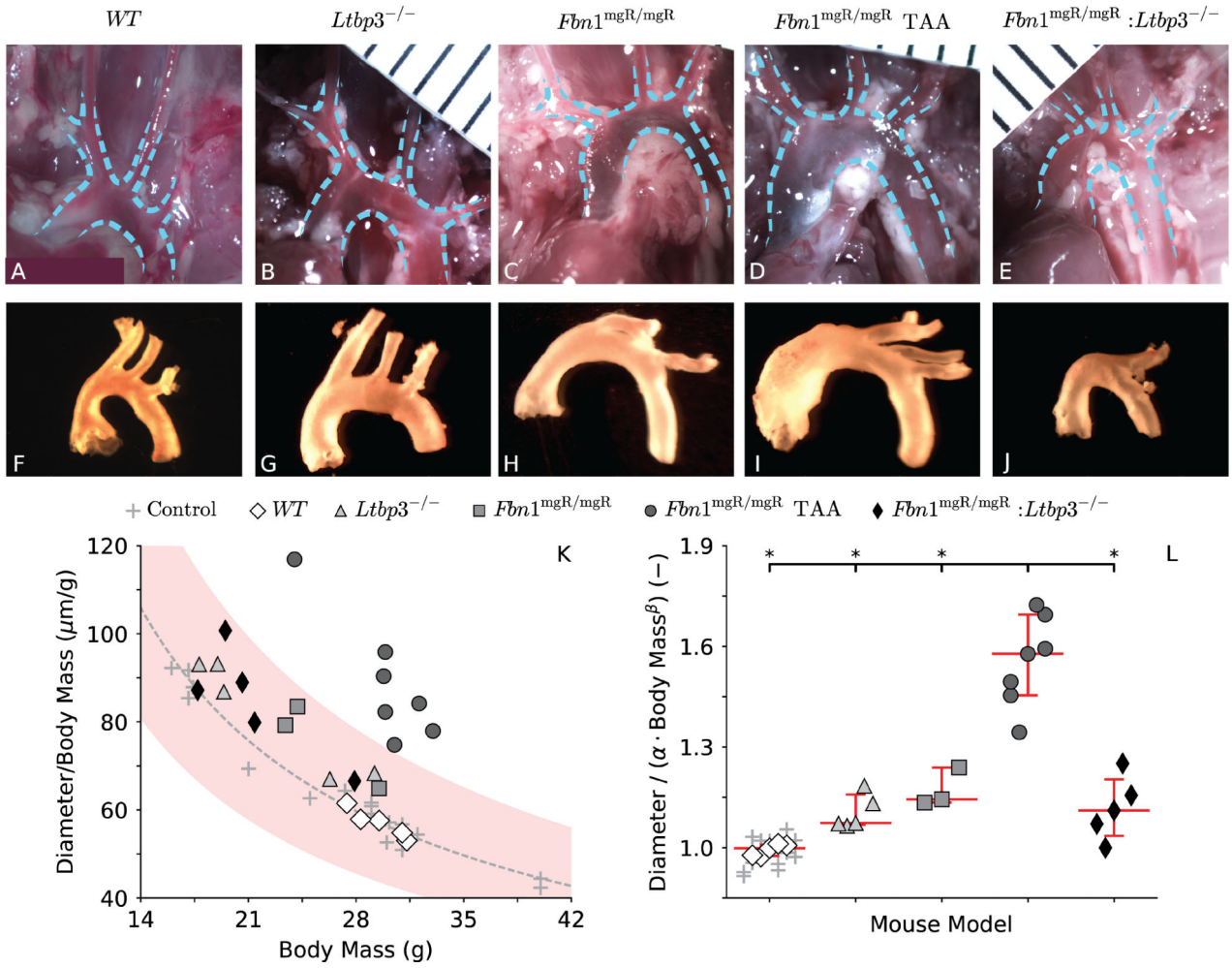

Figure 1.

Configurations of the ascending thoracic aorta (ATA) in situ (A-E) and in vitro following blunt excision (F-J) for all four genotypes: wild-type control (*WT*), LTBP-3 null ($Ltbp3^{-/-}$), fibrillin-1 deficient ($Fbn1^{mgR/mgR}$) without or with aneurysm (TAA), and double mutant ($Fbn1^{mgR/mgR}$:$Ltbp3^{-/-}$). Aortic root, ascending thoracic aorta, major aortic branches, and proximal descending thoracic aorta are outlined in the images taken in situ. While the aortic root in the representative $Fbn1^{mgR/mgR}$ TAA is clearly aneurysmal, the phenotype of the $Fbln1^{mgR/mgR}$:$Ltbp3^{-/-}$ aorta appears close to normal upon gross examination. More rigorously, absence of aortic dilatation in double mutant specimens is revealed by their adherence to a normal allometric scaling law $\hat{d}_{P_{sys}} = \alpha \cdot M^{\beta} = 936.17 \cdot M^{0.17}$ for the systolic inner dimeter of the ATA ($d_{P_{sys}}$) and body mass (M) of control mice (see supplemental Figure S1). The estimated allometric equation predicts the expected ratio $\hat{d}_{P_{sys}}/M$ as a function of M (K, gray dashed line), to which the experimental ratio $d_{P_{sys}}/M$ is compared for each of the current specimens and prior controls (K, gray crosses, used to estimate the allometric parameters). To evaluate how closely the diameter of each specimen ($d_{P_{sys}}$)

matches the value predicted by normal allometric scaling ($\hat{d}_{P_{sys}}$), the ratio $d_{P_{sys}}/\hat{d}_{P_{sys}}$ (is also computed for each specimen (L). Only *Fbn1*$^{mgR/mgR}$ TAA specimens fall outside the 95% confidence interval (K, shaded area) for normal allometric scaling, confirming that absence of LTBP-3 attenuates the aneurysmal dilatation in the mgR mutant mouse. Images in panels A-J are not scaled the same, but are shown for qualitative utility. Statistical significance is set to *$p < 0.05$.

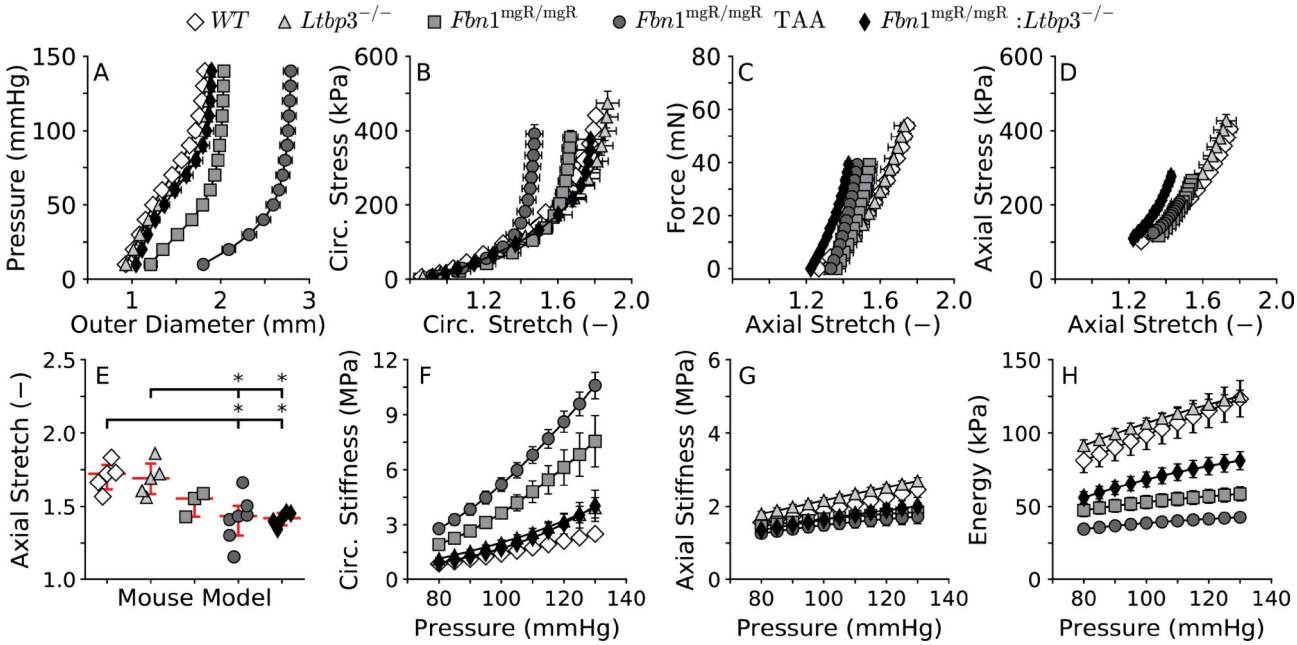

Figure 2.

Biaxial mechanics (A-D) and computed mechanical metrics (E-H) for the considered ATAs, with values of material circumferential (F) and axial (G) stiffness, and energy storage (H) at specimen-specific values of in vivo axial stretch (E) shown over a range of transmural pressures. Note that the pressure-diameter response clearly delineates aneurysmal (TAA) from pre-aneurysmal ATAs (A). Also, note the near full rescue of the circumferential, but not axial, properties in the double mutant ATAs. Consistently, absence of LTBP-3 does not fully recover the stored elastic energy, which depends on both circumferential and axial properties, suggesting that overall vascular function is not fully rescued in $Fbn1^{mgR/mgR}$:$Ltbp3^{-/-}$ specimens. Statistical significance is set to *p < 0.05 for the axial stretch, whereas statistical differences in the pressure-dependent metrics, in unloaded and two loaded configurations (P=100 mmHg and P=120 mmHg), are reported in Table S1.

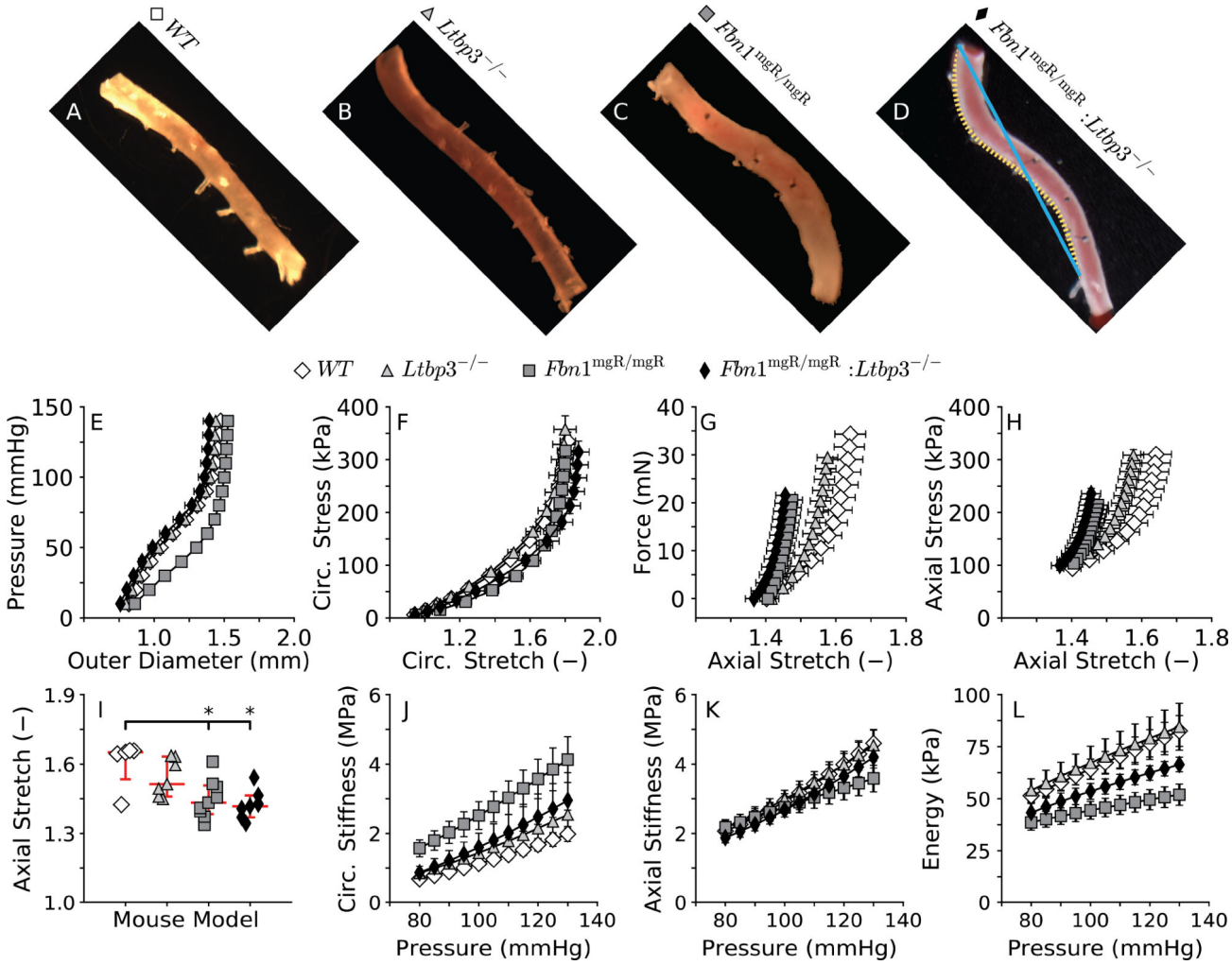

Figure 3.

Configurations of the descending thoracic aorta (DTA) in vitro following blunt excision (AD) for all four genotypes: wild-type control (*WT*), LTBP-3 null ($Ltbp3^{-/-}$), fibrillin-1 deficient ($Fbn1^{mgR/mgR}$), and double mutant ($Fbn1^{mgR/mgR}$:$Ltbp3^{-/-}$). Note that the mgR mutation seems to induce an abnormal curvature of the excised DTA, which can be evaluated by comparing the contour length of the vessel (D, orange dotted line) to the end-to-end distance (D, blue solid line). Albeit informative, gross anatomical descriptors of vascular structure are qualitative and must be complemented with mechanical characterization from biaxial data (E-H) and derived mechanical metrics (I-L). Again, values of material circumferential (J) and axial (K) stiffnesses, and energy storage (L) are evaluated at specimen-specific values of the in vivo axial stretch (I) and shown over a range of transmural pressures. Note that $Fbn1^{mgR/mgR}$ DTAs have a significantly altered pressure-diameter response despite a seemingly normal diameter (E). Similar to findings for the ATA, note the nearly full rescue of the circumferential, but not axial, properties in the double mutant DTA. Statistical significance is set to $*p < 0.05$ for the axial stretch whereas statistical differences in the pressure-dependent metrics, in unloaded and two loaded configurations (P=100 mmHg and P=120 mmHg), are reported in Table S2.

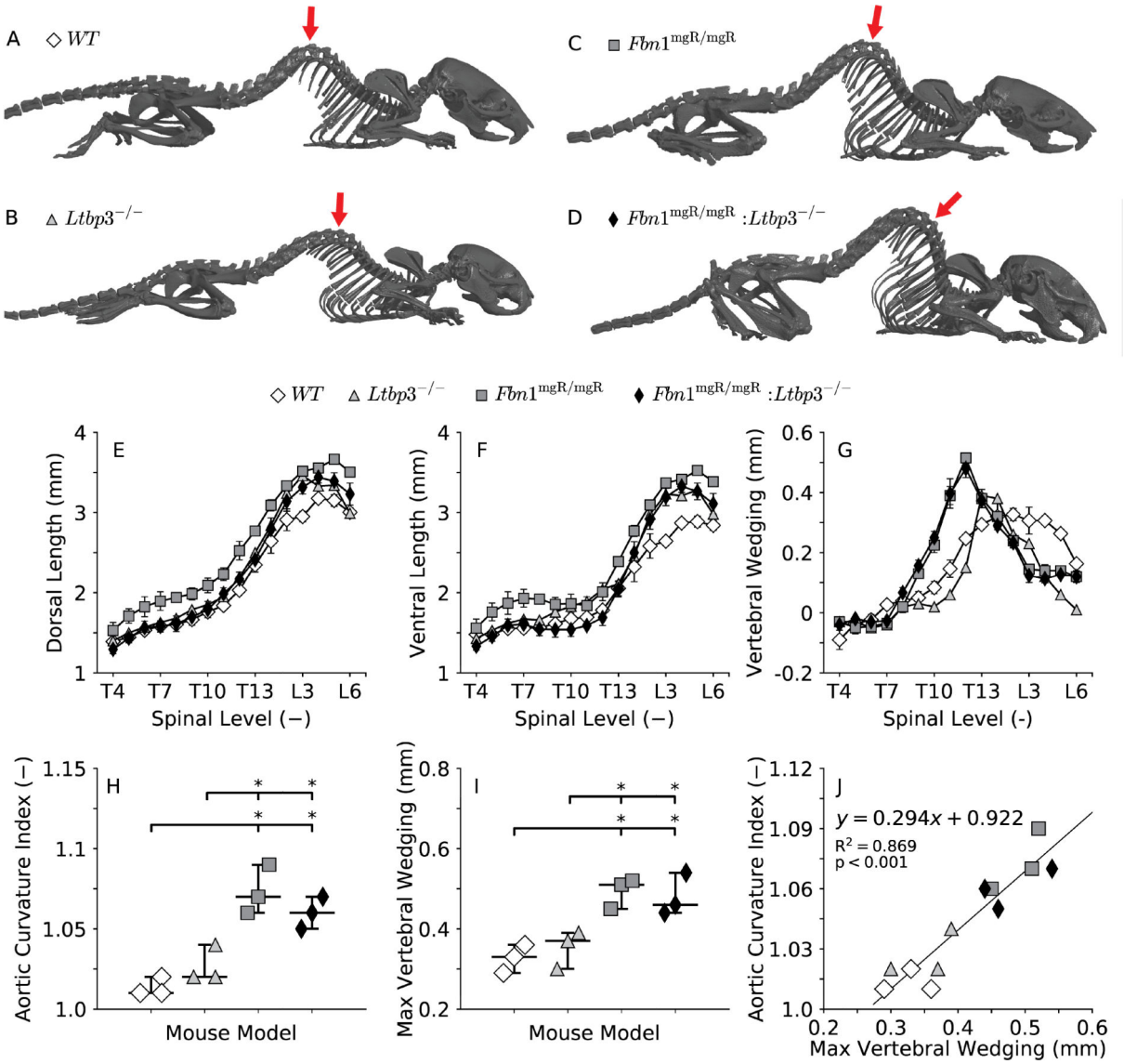

Figure 4.

Representative images of skeletal reconstructions for all four genotypes (A-D). Note that the mgR mutation, even in the absence of LTBP-3, predisposes to excessive thoracic kyphosis, which might be related to the abnormal residual shape of the DTA in *Fbn1*$^{mgR/mgR}$ and *Fbn1*$^{mgR/mgR}$:*Ltbp3*$^{-/-}$ mice (Figure 3, C-D). The severity of thoracic kyphosis is measured in a position-independent manner (Li et al. 2017) through ventral wedging of the vertebrae (G), calculated as the difference between the dorsal (E) and the ventral (F) length of the vertebral bodies in the thoracic (vertebrae T4-T13) and lumbar (vertebrae L1-L3) spine. The aortic curvature index (H), calculated as the ratio of the contour length to the end-to-end distance between the left subclavian and the sixth pair of intercostal arteries (Figure 3, D), quantifies the extent to which the profile of control and mutant DTAs deviates from a straight line. Maximum spinal wedging (I), that is, the maximum difference between the lengths of the dorsal and ventral aspects of the vertebrae (G), quantifies the maximum degree of spinal deformity in the thoracic (vertebrae T4-T13) and lumbar (vertebrae L1-L3)

spine (its anatomical location shown by red arrows in panels A-D). The deviation of the DTA from a straight line (H) and kyphosis of the thoracic spine (I) are more pronounced in both the *Fbn1*$^{mgR/mgR}$ and *Fbn1*$^{mgR/mgR}$:*Ltbp3*$^{-/-}$ mice than in the control mice. In fact, a strong significant correlation exists between these two parameters (J), suggesting that the configuration of the growing spine influences the natural shape of the aorta. Statistical significance is set to *$p < 0.05$.

Table 1.

Best-fit values of the material parameters used to fit the biaxial mechanical data and thus to compute biaxial stress, material stiffness, and stored energy for the *Ltbp3*$^{-/-}$ and Fbn1$^{mgR/mgR}$:*Ltbp3*$^{-/-}$ vessels. Values of the parameters for *WT*, *Fbn1*$^{mgR/mgR}$, and aneurysmal *Fbn1*$^{mgR/mgR}$ (TAA) aortas are reproduced from (Bellini et al. 2016) for convenience.

	Elastic Fibers	Axial Collagen		Circumferential Collagen + SMC		Symmetric Diagonal Collagen			Error
	c (kPa)	c_1^1 (kPa)	c_2^1	c_1^2 (kPa)	c_2^2	$c_1^{3,4}$ (kPa)	$c_1^{3,4}$	α_0 (deg)	RMSE
ATA									
Ltbp3$^{-/-}$	39.856	19.266	0.080	0.005	1.182	5.813	0.363	47	0.059
Fbn1$^{mgR/mgR}$:*Ltbp3*$^{-/-}$	45.822	28.206	0.312	0.035	1.194	5.737	0.871	41	0.049
WT	43.993	14.978	0.028	7.590	0.234	6.476	0.426	44	0.048
Fbn1$^{mgR/mgR}$	23.102	12.988	0.230	0.009	2.389	7.478	0.747	47	0.068
Fbn1$^{mgR/mgR}$ TAA	21.687	11.139	0.005	8.44E^{-05}	8.289	11.138	1.555	50	0.092
DTA									
Ltbp3$^{-/-}$	36.546	10.666	0.451	7.380	0.236	0.073	2.212	31	0.070
Fbn1$^{mgR/mgR}$:*Ltbp3*$^{-/-}$	27.564	10.662	0.929	3.929	0.197	0.033	3.144	29	0.082
WT	31.944	13.496	0.163	11.213	0.146	0.097	1.816	27	0.054
Fbn1$^{mgR/mgR}$	29.040	1.293	1.778	1.139	0.577	0.338	2.384	29	0.084